Desalination and Water Treatment
www.deswater.com

doi: 10.5004/dwt.2021.27843

242 (2021) 106–116
December

Inhibition of copper alloy corrosion using CBG-HCl as a green inhibitor in 0.5 M H_2SO_4 solution

Abdualah Elhebshi[a], Ahmed El Nemr[b,*], Mohamed S. El-Deab[c], Ibrahim Ashour[a,d], Safaa Ragab[b]

[a]*Chemical Engineering Department, Faculty of Engineering, Elminia University, Elminia, Egypt, emails: hebshi71@gmail.com (A. Elhebshi), ibrahim.ashour@gmail.com (I. Ashour)*
[b]*Environmental Division, National Institute of Oceanography and Fisheries, NIOF, Kayet Bey, El-Anfoushy, Alexandria, Egypt, emails: ahmedmoustafaelnemr@yahoo.com/ahmed.m.elnemr@gmail.com (A. El Nemr)*
[c]*Department of Chemistry, Faculty of Science, Cairo University, Cairo, Egypt, email: msaada68@yahoo.com*
[d]*Zewail City, University of Science and Technology, 6th October City, Giza, Egypt*

Received 22 February 2021; Accepted 25 September 2021

ABSTRACT

This study investigates the activity of hydrochloride salt of chitosan biguanidine (CBG-HCl) as a green corrosion inhibitor of copper alloy in 0.5 M H_2SO_4 solution. The obtained results from both the potentiodynamic and electrochemical impedance spectroscopy analyses reported a noticeable increase in the corrosion inhibition of copper alloy in 0.5 M H_2SO_4 solution in the presence of CBG-HCl. The presence of CBG-HCl in the corrosive solution may block the copper alloy's pores on the outer surface, preventing the corrosive gradients from reacting with the surface of the copper alloy. An inhibition efficiency (IE) of 85% is achieved in the presence of 200 ppm CBG-HCl. Moreover, potentiodynamic experiments indicated that CBG-HCl acted as an anodic inhibitor that reduced partial anodic reaction to corrosion of studied copper alloy in 0.5 M H_2SO_4. IE of CBG-HCl remains effective during a long exposure time which proved the high stability of CBG-HCl inhibitor in 0.5 M H_2SO_4.

Keywords: Copper alloy; Electrochemical impedance spectroscopy; Chitosan biguanidine hydrochloride; Green corrosion inhibitor; Modified natural polymer

1. Introduction

Copper is a widely utilized metal in the industry due to its mechanical properties and excellent electrical and thermal conductivities [1,2]. While copper alloys have relatively noble properties in a dry atmosphere, they corrode in alkaline and acidic solutions [3]. This limits the use of copper alloys in many applications, such as the cooling and heating system in desalination units, especially thermal distillation units, and other industrial applications [4–7].

Corrosion inhibitors are widely used to decrease the corrosion rate of metal in oil and industry processes when using acid cleaning processes such as acid beading processes, acid purification in industry, and acidification of oil and gas wells for rust and scale removal [8–13]. The defense of inhibitors primarily focuses on absorbing inhibitor compounds and the subsequent creation of a protective layer for modifying metal surfaces. Many corrosion inhibitors used were natural compounds that mainly contain heterogeneous atoms that improve the adsorption on the metal surface, such as nitrogen, sulfur, phosphorus, and oxygen. These natural organic compounds were used as green inhibitors for metals corrosion [14–16]. In this context, many researchers have shifted the vision to natural plant extracts or

* Corresponding author.

medicines that humans often use to treat various diseases to develop environmentally-friendly corrosion inhibitors [17–23]. The global health and environmental pollution issues caused by several inhibitor categories have targeted the production of cheap, efficient, low- or null-negative green corrosion inhibitor molecules [12–16,24,25].

Heating and cooling systems are an essential part of thermal distillation units, a new trend to improve water sources. The thermal distillation unit is divided into different stages; each stage consists of a suitable metal for its work. One of these stages is condenser tubes which are mainly made of copper alloys. After a certain period of about 110 d, the unit must be stopped for reducing scales formed due to thermal evaporation of seawater to keep heat transfer proficiency. The industrial practice of acid cleaning originally emanated from developing technology for improving stages capability and dissolving surface scales and deposits. And the acid cleaning involves the use of highly reactive acids such as sulfuric acid (H_2SO_4) [26–29]. Acid should be injected into the system and circulated for 6–8 h and need a long corrosion study period than 8 h [30].

The natural biopolymer chitosan organic compound (COC) was investigated in molar hydrochloric acid as a copper corrosion inhibitor by Jmiai et al. [31]. This research was conducted out using accurate weight loss measurements and electrochemical measurements. To describe the surface of metal specimens, uninhibited and inhibited may be used. Many instruments can be used for surface analysis, such as scanning electron microscopy (SEM), energy-dispersive X-ray spectroscopy (EDX), and atomic force microscopy (AFM). The study of the temperature effect showed the adsorption's chemical nature. The experimental inhibition efficiency calculated by different electrochemical and gravimetric analyses was confirmed by computational chemistry and the inhibition efficiency of various chemical compounds [32–38]. Solomon et al. [39] investigated the inhibitory capability of chitosan alone with KI of stainless steel St37 in the 15% H_2SO_4 solution using potentiodynamic polarization (PDP), electrochemical impedance spectroscopy (EIS), dynamic electrochemical impedance spectroscopy (DEIS) and weight loss (WL). And this was complemented by a morphological surface exam using SEM and EDX. Fekry et al. [40] prepared the acetyl thiourea chitosan polymer (ATUCS) and investigated it as a mild steel corrosion inhibitor in 0.5 M H_2SO_4 acid. ATUCS have demonstrated an excellent inhibition efficiency (IE) (94.5%) in 0.5 M solution of sulfuric acid containing 0.76 mM of ATUCS. The previous literature investigated the effect of the types and concentrations of diluted acid media on the relationship between the structure and properties of chitosan for 5 h. The properties and structure of chitosan are directly affected by protonation, and the performance of HCl-modified film is very good at room temperature. Still, after 5 h and by rising temperature more than room temperature, chitosan will be degraded. The degraded chitosan will be slightly affected by the corrosion mechanism or may not be an effective inhibitor in the highly corrosive and strong acids used in the acid cleaning process. And no film will be fabricated on a metal surface [41].

Generally, the following two steps are essential in acid hydrolysis of chitin/chitosan: the hydrolysis of the glycosidic linkages (main chain scission) and hydrolysis of N-acetyl linkages (side chain scission). The hydrolysis of the glycosidic linkages is SN1 reaction, whereas the hydrolysis of *N*-acetyl linkages is SN2 reaction. At a temperature more than room temperature and in the presence of a high percentage of acid, both processes (scission of glycosidic links and scission of *N*-acetyl groups) occurred simultaneously. The macromolecules may decay into monomers, acetic acid, and other small molecules. The degradation condition is very aggressive, and the energy required to break the two linkages is achieved at high temperatures. Reactions were performed as before, except that the final HCl concentration was wide-ranging between 0.1 and 1.0 M and the reaction was terminated after 5 h [42,43].

From the previous knowledge, our team decided to study the hydrochloride salt of chitosan biguanidine (CBG-HCl, a modified natural polymer), as a vertebral corrosion inhibitor of copper alloy in 0.5 M H_2SO_4 medium at room temperature and measure expose time of 400 min as a maximum period of acid cleaning. Also, we measure the IE and clarify the most applicable adsorption isotherm of CBG-HCl as a green corrosion inhibitor of copper alloy in 0.5 M H_2SO_4.

2. Experimental

2.1. Solutions and chemicals

H_2SO_4 was obtained from Fluka (98%) and used as received. The corrosive solution (electrolyte, 0.5 M H_2SO_4) was prepared at the concentration needed by diluting concentrated sulfuric acid using deionized water.

2.2. Preparation of CBG-HCl inhibitor

Hydrochloride salt of chitosan biguanidine (CBG-HCl) (Fig. 1) was produced based on literature as a modified natural polymer [13,44–46]. 10 g of commercial chitosan (Aldrich) were dissolved by stirring in 500 mL of 1 N HCl at 80°C for 1 h; then 5.72 g of cyanoguanidine in water (100 mL) was added to the acidic solution of chitosan. The reaction mixture was refluxed for 5 h at 100°C, the reaction mixture was cooled to room temperature, followed by precipitation with excess ethanol. By filtration, the white precipitate was collected, washed with ethanol, and oven-dried at 50°C to provide 17.95 g (90.60%). By comparing its analysis with the reported literature analysis, the CBG-HCl structure was confirmed [13,44–46].

2.3. Electrochemical, copper alloy, corrosion cell and equipment

The working electrode was a rod of copper alloy (wt.%): 0.9 Ca, 0.2 Sn, 0.1 Mo, 0.8 Fe, 31.4 Zn, 66.6 Cu. The copper rod was screened with a Teflon coat, leaving an exposed two-dimensional area of 0.8 cm^2. The counter and reference electrodes were the saturated calomel electrode (SCE) and a graphite rod (1 cm diameter × 15 cm long), respectively. A three-electrode glass cell was applied for electrochemical calculation using a potentiostat/galvanostat (Gamry series-G 300 model) using Gamry Fram work version 6.12. Impedance measurements were conducted at a frequency range between 0.1 Hz and 100 kHz with a

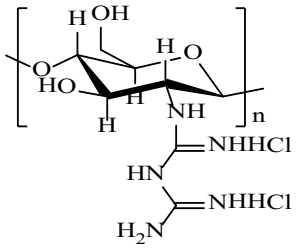

Fig. 1. CBG-HCl chemical structure.

peak-to-peak amplitude of 10 mV using AC signals under open circuit potential (OCP) for copper alloy rod conditions. The impedance spectrum was analyzed with the software Equivalent Circuit.

2.4. Methodology of experiments

The copper alloy working electrode was polished with SiC wet paper before each test. Then washed with distilled water, rubbed with ethanol in an ultrasound bath and dried well before immersing in the corrosive medium, which is 0.5 M sulfuric acid containing different amounts of CBG-HCl. The electrolyte was made from water and analytical chemicals that were distilled. The geometrical surface of the working electrode of the copper alloy refers to all the information (current, impedance, resistance) recorded in this study. Electrochemical tests were performed at 25°C ± 2°C. EIS and polarization analyses were performed by immersing the working electrode for approximately 30 min in the test media, following a steady free corrosion potential value. The polarization curves were determined at a scan rate of 5 mV s^{-1} (approximately –250 mV vs. OCP) from the OCP to the cathodic direction. Then the possible scan was reversed to approximately final potential +250 mV relative to OCP. All experimental work was repeated at least three times, and only mean values with ±1.2 standard deviation were recorded here.

3. Results and discussion

3.1. Electrochemical impedance spectroscopy analysis

EIS experiments were performed to determine the IE of corrosion of CBG-HCl for the copper alloy electrode surface in 0.5 M H_2SO_4 media. EIS analyses were performed at OCP in a broad frequency range between 0.10 Hz and 100 kHz, with an AC voltage amplitude of ±10 mV. The copper alloy electrode was stabilized for 30 min at OCP until analyses were made at 25°C ± 2°C. The EIS data outlined in Fig. 2 as a Nyquist diagram for blank and the different CBG-HCl concentrations (25, 50, 100, 150 and 200 ppm), reported on a copper alloy electrode in the corrosive medium. Fig. 2 shows that the semicircle diameter increases with an increase in the concentration of the inhibitor in the electrolyte, indicating that the inhibitor can form adsorption on the copper alloy surface, which increases the corrosion resistance of the copper.

The electrical equivalent circuit (EEC) illustrated in Fig. 3a may be simulated the EIS data and used to measure equivalent resistance [47]. The inhibitor efficiency at different concentrations was calculated using Eq. (1) and reported in Table 1 [48–53]. R_{el} is the ohmic solution resistance between the reference electrode and the working electrode. In EEC; R_1 is the metal resistance with the corrosion reaction at OCP; CPE1 is the constant phase element of the electrical double-layer at the electrode/electrolyte interface. R_2 is the pseudo-resistance of the surface-adsorbed inhibitor layer, whereas CPE2 is the constant phase element of the adsorbed layer. The sum of $R_1 + R_2$ represents the total resistance in the presence of CBG-HCl. Fig. 3b and c present EEC model sample fitting in the absence and CBG-HCl presence.

$$\mathrm{IE}\% = \left(1 - \left[\frac{R_p^{(b)}}{R_p^{(\mathrm{in})}}\right]\right) \times 100 \quad (1)$$

where $R_p^{(b)}$ and $R_p^{(\mathrm{in})}$ are the polarization resistances in the absence and the presence of the inhibitor, respectively.

A significant improvement in the performance of copper alloy IE with an increase in electrolyte inhibitor concentration is shown in Table 1. The increase in polarization resistance values ($R_1 + R_2$) is evident in this improvement in IE. With 200 ppm of CBG-HCl, the maximum IE value (85.11%) was achieved.

3.2. Potentiodynamic measurements

Potentiodynamic tests have been performed to validate the data obtained from EIS measurements. To achieve a non-linear Tafel plot between E(volt) and Im(A cm^{-2}) where Im = current, potential range from –0.25 to +0.25 V concerning OCP is applied. OCP was measured using a saturated calomel electrode as a reference electrode. Fig. 4 records potentiodynamic polarization curves of a copper alloy electrode in a 0.5 M H_2SO_4 solution at different CBG-HCl concentrations in the electrolyte. From the slope of the a-axis and b-axis, we can calculate anodic and cathodic slopes of Tafel (β_a and β_c, respectively). Also, from the intercept of the two axes, E_{corr} and I_{corr} can be calculated Table 2. The results show a clear decrease in the anodic current associated with the increase of the inhibitor concentration (anodic branch shifted below) in the solution. CBG-HCl is an anodic inhibitor, reducing the partial anodic corrosion reaction. Eq. (2) [54,55] was used to calculate IE.

$$\mathrm{IE}\% = \left(1 - \frac{i_{\mathrm{in}}}{i_b}\right) \times 100 \quad (2)$$

The corrosion current at a given concentration of the inhibitor is i_{in} (A cm^{-2}) and i_b is the corrosion current in the blank solution in the absence of an inhibitor.

Fig. 5 shows the mean inhibition efficiency values with the standard deviation obtained using the results of both EIS and potentiodynamic experiments at different inhibitor concentrations (25, 50, 100 and 200 ppm) in the electrolyte.

3.3. Adsorption isotherm

Freundlich, Temkin, and Langmuir isotherm models were conducted to describe the absorption of CBG-HCl on

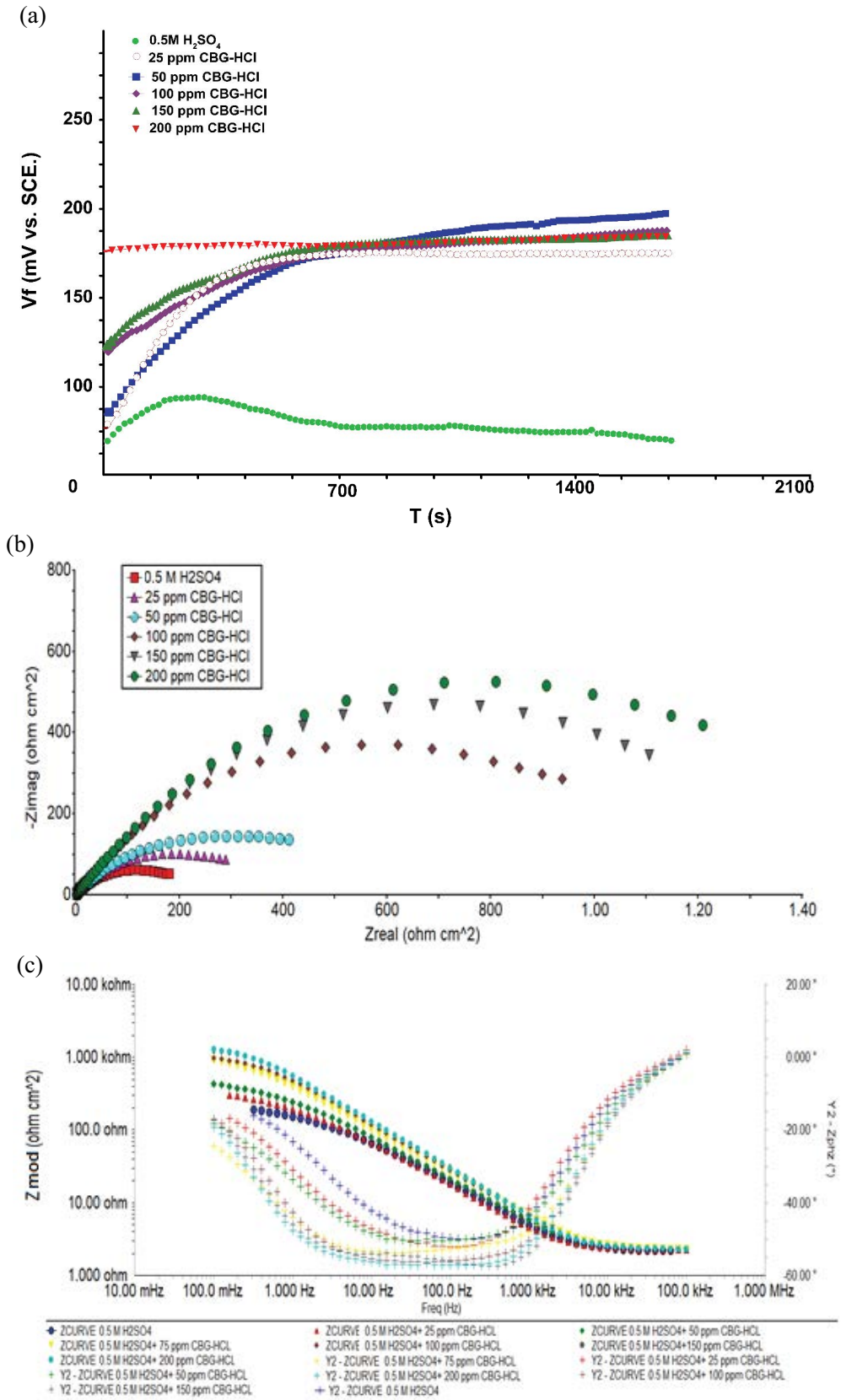

Fig. 2. (a) Open circuit potential, (b) Nyquist and (c) bode of the copper alloy plot obtained at various CBG-HCl levels in 0.5 M H_2SO_4 at 25°C ± 2°C.

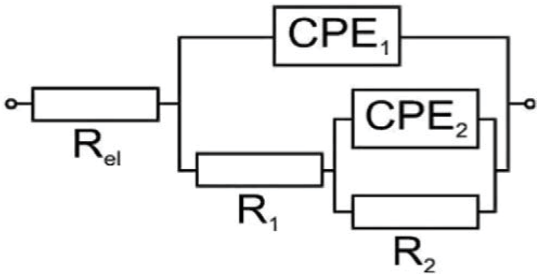

(a)

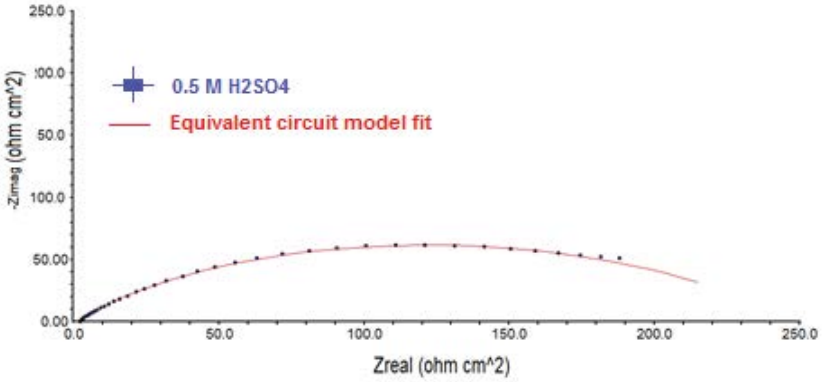

(b)

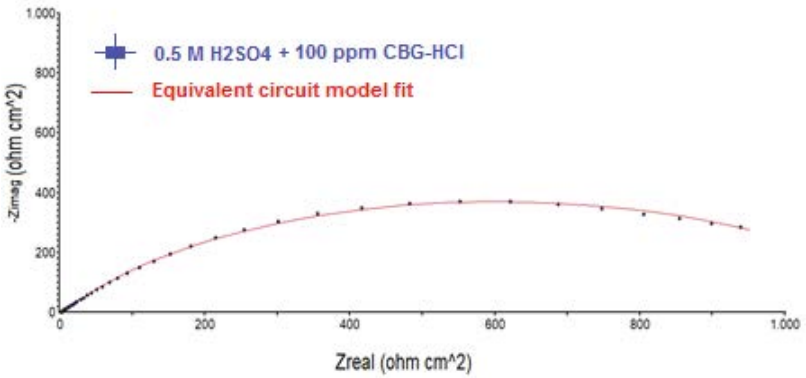

(c)

Fig. 3. (a) The EEC model was used to simulate EIS data obtained on copper alloy electrodes immersed in 0-containing electrolytes and different inhibitor concentrations. Where R_{el}, R_1, R_2, CPE1 and CPE2 represent solution resistance, charge transfer resistance, pseudo-resistance of the surface-adsorbed inhibitor layer, the capacitance of double-layer and pseudo-capacitance, respectively. The model fitting in (b) absent and (c) presence of 100 ppm CBG-HCl.

Table 1
Current equivalent circuit parameters and calculated IE of different inhibitor concentrations

Electrolyte composition	R_{el} (Ω cm^2)	$R_1 + R_2$ (Ω cm^2)	CPE1 × 10^6 (Ω^{-1} cm^{-2} S$^{\alpha}$)	CPE1 × 10^6 (Ω^{-1} cm^{-2} S$^{\alpha}$)	α_2	α_2	IE%
Blank (0.5 M H_2SO_4) (A)	0.672	246.8	1,147	133	0.905	0.89	–
A + 25 PPM CBG-HCl	0.541	403.8	1,087	120	0.877	0.79	38.88
A + 50 PPM CBG-HCl	0.591	578	971	105	0.899	0.81	57.30
A + 100 PPM CBG-HCl	0.438	1,217	374	93	0.866	0.68	79.72
A + 150 PPM CBG-HCl	0.527	1,456	325	70	0.848	0.91	83.05
A + 200 PPM CBG-HCl	0.510	1,658	305	56	0.704	0.85	85.11

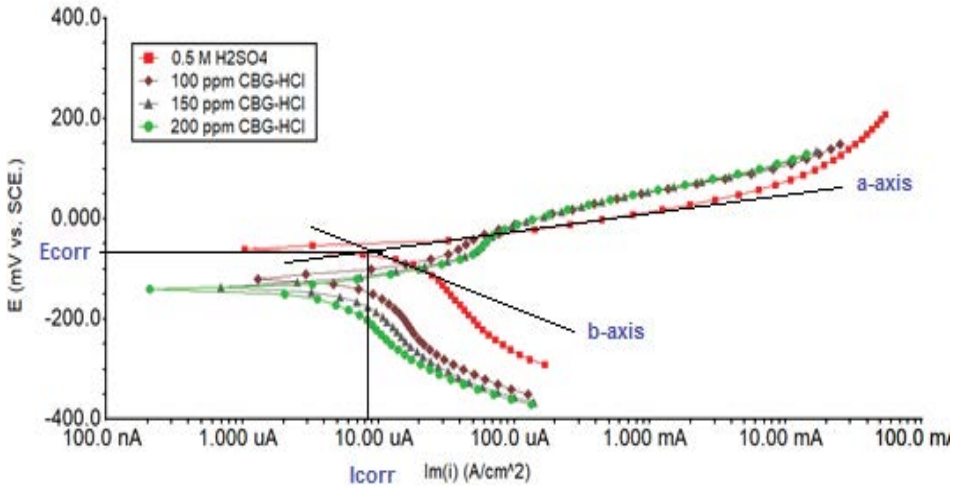

Fig. 4. Copper alloy electrode potentiodynamic graphs were recorded at different CBG-HCl concentrations in a 0.5 M H_2SO_4 solution.

Table 2
Explains corrosion current density (I_{corr}), the cathodic and anodic slopes of Tafel (β_c and β_a, respectively), the corrosion potential (E_{corr}) in a 0.5 M H_2SO_4 solution containing different CBG-HCl concentrations and the corresponding efficiency values of corrosion inhibition

Electrolyte composition	$-E_{corr}$ (mV vs. SCE)	Current density of corrosion (I_{corr}) (mA cm^{-2})	β_a (mV dec^{-1})	β_c (mV dec^{-1})	IE (%)
Blank (0.5 M H_2SO_4) (A)	60.7	0.024	0.043	0.770	–
A + 25 ppm CBG-HCl	43	0.015	0.042	0.099	37.5
A + 50 ppm CBG-HCl	64.7	0.012	0.066	0.085	50.0
A + 100 ppm CBG-HCl	95.8	0.009	0.076	0.168	62.51
A + 150 ppm CBG-HCl	134	0.007	0.067	0.333	70.83
A + 200 ppm CBG-HCl	142	0.005	0.065	0.287	79.17

the copper alloy surface. The Langmuir isotherm model agrees with the obtained results, which assumes that the IE is proportional to the CBG-HCl surface coverage θ [48,56]. The mean corrosion IE values obtained using the two electrochemical experimental techniques (Fig. 5) are shown in Fig. 6 in the form of a linearized Langmuir isotherm by equation (3) [48,49].

$$\frac{C}{\theta} = \frac{1}{K_{ads}} + C \tag{3}$$

where C is the concentration of the inhibitor, θ is the surface coverage, and K_{ads} is the constant of adsorption equilibrium. If the plot of C/θ vs. C is linear and the slope of the line is close to unity, an inhibitor is considered to follow Langmuir. Similar results were obtained for Temkin and Freundlich isotherms. The Langmuir isotherm shows high correlation coefficients (R^2) obtained from plots (Fig. 6) and reported in Table 3 as $R^2 = 0.9954$ and slope is 1.015. On the copper alloy surface, this implies monolayer inhibitor adsorption.

The constant K_{ads} = 0.0229 dm^3 mg^{-1} (L mg^{-1}) was obtained from Fig. 6, and the corresponding standard Gibbs free energy (ΔG°_{ads}, kJ mol^{-1}) was obtained from Eq. (4) [48,50,51,56,57].

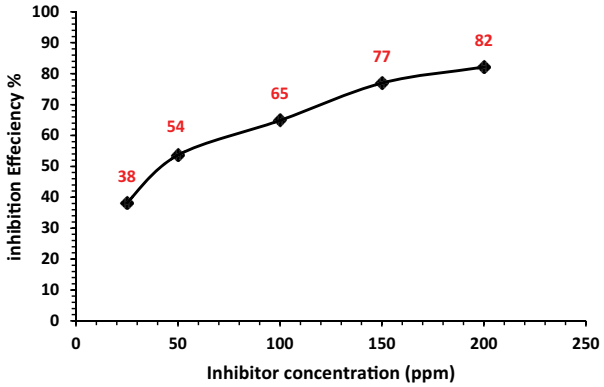

Fig. 5. The efficiency of average corrosion inhibition values of CBG-HCl on Cu alloy in 0.5 M H_2SO_4 solution obtained by EIS and potentiodynamic experiments.

$$K_{ads} = \frac{1}{C_{solvent}} \exp\left(\frac{-\Delta G^0_{ads}}{RT}\right) \tag{4}$$

where T is the absolute temperature (K), $C_{solvent}$ is the solvent molar concentration (C_{H_2O} = 10^6 mg dm^{-3}), and the

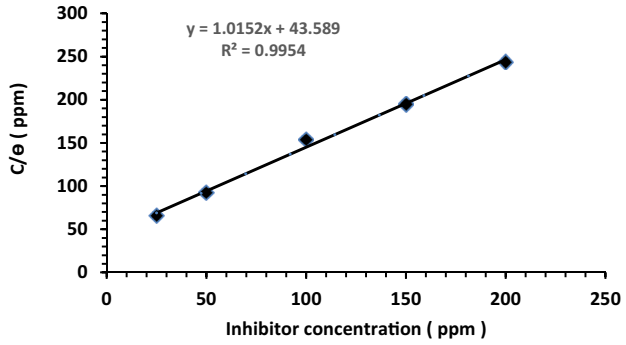

Fig. 6. Langmuir isothermal plot for CBG-HCl adsorption in the corrosive medium on the surface of Cu alloy.

Table 4
Dependence of time-based inhibition efficiency and corrosion resistance from EIS measurements obtained on a copper alloy electrode in a 0.5 M H_2SO_4 solution in the presence of 200 ppm CBG-HCl

Time (min)	R_p (ohm cm^{-2})	IE%
	In present of 200 ppm CBG-HCl	
30	1,660	85.13
60	1,750	85.90
120	1,760	85.98
240	1,680	85.31
360	1,754	85.93

Data was collected at selected time intervals.

gas constant is R (J mol^{-1} K^{-1}). The Gibbs free of CBG-HCl adsorption energy on the surface of the copper alloy was –24.8 kJ mol^{-1} at 298 K. Literature shows that charge sharing between molecules and metal (chemisorption) implies magnitudes of standard Gibbs free adsorption energy in aqueous solution around or higher (more negative) than –40 kJ mol^{-1}, while around –20 kJ mol^{-1} or lower indicates adsorption between adsorbent and adsorbate (physisorption) with electrostatic interaction [58–60]. The corresponding calculated value of standard Gibbs free adsorption energy (–24.8 kJ mol^{-1}) shows that physisorption is the adsorption of CBG-HCl and the negative values of $-\Delta G^{\circ}_{ads}$ ensure the spontaneity of the adsorption process and the stability of the copper alloy surface adsorbed layer.

3.4. Impact of time on the efficiency of the inhibitor

Experiments were conducted at different interval times to evaluate the time required for the inhibitor to achieve optimum IE and stability using EIS under test conditions in the presence of 200 ppm CBG-HCl in 0.5 M H_2SO_4 solution. Both Table 4 and Fig. 7 introduce the corresponding values of IE and corrosion resistance. The data shows that the corrosion inhibition efficiency reached 85% within 30 min after immersion of the copper alloy electrode in the electrolyte. After 2 h of testing, the maximum efficiency (85.98%) was reached and remained as high as 85.93% after 6 h.

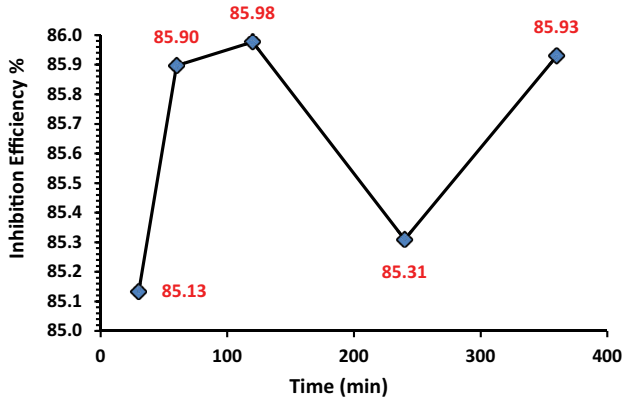

Fig. 7. Inhibition efficiency in the presence, at selected time intervals, of 200 ppm CBG-HCl in a 0.5 M H_2SO_4 solution resulting from EIS experiments performed on copper alloy electrodes.

3.5. Surface morphology study by SEM

The surface of the copper samples was immersed without and in the presence of 200 ppm of (CBG-HCl). After retrieving the samples, following the drying steps, the surface morphology was inspected using SEM. The results in the form of the SEM images displayed in Fig. 8a–c for the blank before 0.5 M H_2SO_4, after immersion two weeks in 0.5 M H_2SO_4, and after inhibition by 200 ppm of (CBG-HCl), respectively. From the image of the blank sample, it was evident that it shows considerable damage due to the corrosive attack of the 0.5 M H_2SO_4 solution resulting in several striations and damaged appearance. On the other hand, the inhibited sample by (CBG-HCl) displays an almost smooth metallic surface, which indicates the adsorption and the formation of a protective inhibitor film.

3.6. EDX results and corrosion inhibition mechanism

The results presented demonstrate that CBG-HCl is an effective copper corrosion inhibitor in a 0.5 M H_2SO_4 solution. Potentiodynamic plots result in Fig. 4 shows that the inhibitor works as an anodic inhibitor, reducing the partial reaction of anodic corrosion. Via the donor-acceptor interaction between the lone electron pair on the inhibitor compounds heteroatoms and Cu ions on the metal surface, adsorption on the anodic sites occurs. The mechanism of the inhibition action is to form a protective layer on the copper alloy surface that prevents access to the copper metal surface of corrosive agents by creating a strong hydrocarbon barrier due to the presence of a long hydrocarbon (–CH_2) chain. The protective layer is induced by the adsorption of chloride ions of inhibitor firstly followed by adsorption of the protonated chitosan, Fig. 9. The IE depends on the surface coverage (θ) and the concentration on the metal surface of adsorbed inhibitor molecules. In this context, EDX measurements were carried out on tested copper alloy samples to prove the tightness of the CBG-HCl layer on the copper alloy surface. The EDX outcomes shown in Fig. 10 significant increases in the weight percentage of carbon and oxygen elements

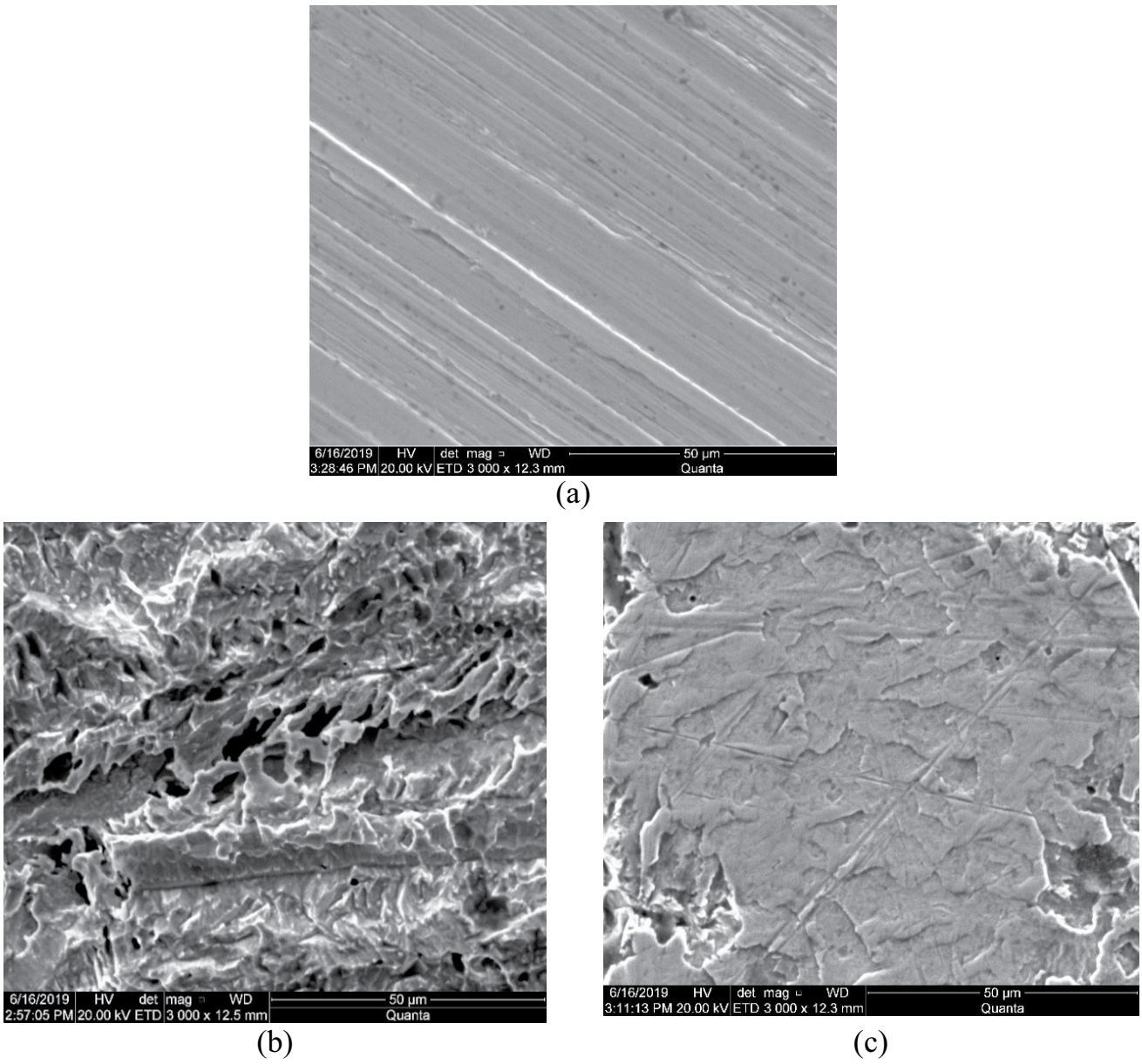

Fig. 8. SEM images of a copper alloy surface taken after two weeks of contact time with 0.5 M H_2SO_4 solution, where (a) is for the fresh copper alloy sample (free of solution), (b) is in the blank solution (absence of CBG-HCl), and (c) in the presence of 200 ppm CBG-HCl in the solution.

Table 5
Results of EDX spectra demonstrate the weight percentage of particular sample surface elements obtained for copper alloy after immersion in 0.5 M H_2SO_4 containing CBG-HCl 200 ppm for 24 h

Element	Wt.%	
	Before immersing in an inhibited solution	After immersing in an inhibited solution
Carbon	0.74	1.35
Oxygen	1.00	1.14

(which are the highest content of the inhibitor molecule) on the surface of a 24 h copper alloy sample immersed in 0.5 M H_2SO_4 solution at 200 ppm CBG-HCl are shown in Table 5. The increase in element percentages on the sample surface is proportional to the amount of inhibitor adsorbed on the surface and then to the metal surface coverage.

4. Conclusions

According to the above results, the following could be concluded:

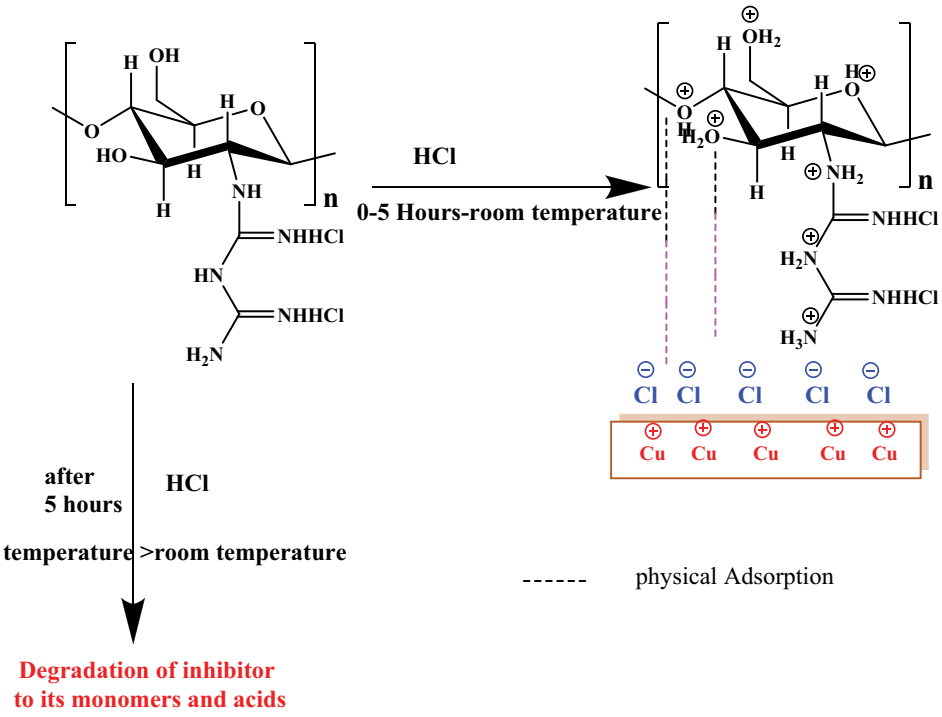

Fig. 9. Investigation of the adsorption mechanism CBG-HCl on the surface of copper alloy in 0.5 M H_2SO_4.

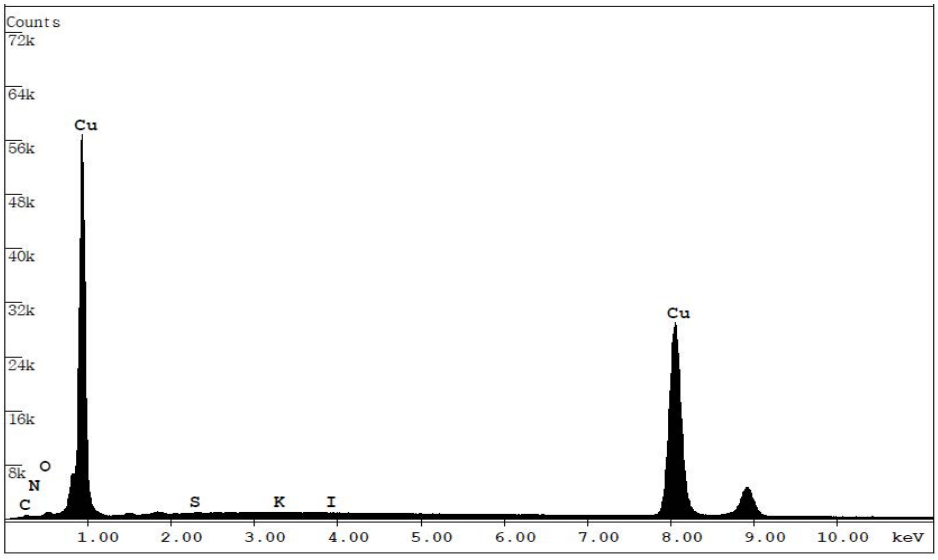

Fig. 10. EDX spectra of copper alloy sample after immersion in 0.5 M H_2SO_4 for 24 h in the presence of 200 ppm CBG-HCl inhibitor.

- The high IE of CBG-HCl on Cu alloy corrosion in acidic solution has been consistently revealed by EIS and potentiodynamic results.
- EIS analyses revealed that the inhibitor gives a proper long-term effective corrosion IE at 200 ppm of CBG-HCl as an inhibitor within different periods of immersion of copper in 0.5 M H_2SO_4 solution.
- Potentiodynamic measurements have shown that the CBG-HCl inhibitor acts as an anodic inhibitor, reducing the partial anodic reaction of corrosion. The inhibition mechanism of the CBG-HCl occurred via forming a surface adsorbed layer, which prevents the access of the corrosive solution to attack the copper alloy surface via forming a hydrophobic barrier due to the hydrocarbon chain in the CBG-HCl.
- The mechanism of inhibitor adsorption following the Langmuir isotherm model and the corresponding negative values of standard Gibbs free energy adsorption suggests that the process is spontaneous and physisorptive.

References

[1] M.S. Hasanin, S.A. Al Kiey, Environmentally benign corrosion inhibitors based on cellulose niacin nano-composite for corrosion of copper in sodium chloride solutions, Int. J. Biol. Macromol., 164 (2020) 3709–3717.

[2] T. Yan, S. Zhang, L. Feng, Y. Qiang, L. Lu, D. Fu, Y. Wen, J. Chen, W. Li, B. Tan, Investigation of imidazole derivatives as corrosion inhibitors of copper in sulfuric acid: combination of experimental and theoretical researches, J. Taiwan Inst. Chem. Eng., 106 (2020) 118–129.

[3] G. Vastag, E. Szocs, A. Shaban, E. Kalman, New inhibitors for copper corrosion, Pure Appl. Chem., 73 (2001) 1861–1869.

[4] L. Zhou, S. Zhang, B. Tan, L. Feng, B. Xiang, F. Chen, W. Li, B. Xiong, T. Song, Phenothiazine drugs as novel and eco-friendly corrosion inhibitors for copper in sulfuric acid solution, J. Taiwan Inst. Chem. Eng., 113 (2020) 253–263.

[5] N. Benzbiria, S. Echihi, M.E. Belghiti, A. Thoume, A. Elmakssoudi, A. Zarrouk, M. Zertoubi, M. Azzi, Novel synthetized benzodiazepine as efficient corrosion inhibitor for copper in 3.5% NaCl solution, Mater. Today:. Proc., 37 (2020) 3932–3939.

[6] R.K. Ahmed, S. Zhang, Bee pollen extract as an eco-friendly corrosion inhibitor for pure copper in hydrochloric acid, J. Mol. Liq., 316 (2020) 113849, doi: 10.1016/j.molliq.2020.113849.

[7] J. He, Q. Li, X. Li, J. An, G. Chen, L. Zhao, W. Li, Insight into the anti-corrosion mechanism of 2-aminobenzenethiol as the inhibitor for copper in acid environment, J. Mol. Liq., 320 (2020) 114494, doi: 10.1016/j.molliq.2020.114494.

[8] X. Zhang, F. Wang, Y. He, Y. Du, Study of the inhibition mechanism of imidazoline amide on CO_2 corrosion of Armco iron, Corros. Sci. 43 (2001) 1417–1431.

[9] M.B. Kermani, A. Morshed, Carbon dioxide corrosion in oil and gas production—a compendium, Corrosion, 59 (2003) 659–683.

[10] A. Asan, S. Soylu, T. Kıyak, F. Yıldırım, S.G. Oztas, N. Ancın, M. Kabasakaloglu, Investigation on some Schiff bases as corrosion inhibitors for mild steel, Corros. Sci., 48 (2006) 3933–3944.

[11] A.B. Shein, A.V. Denisova, Choice of effective corrosion inhibitors for acid treatment of wells, Prot. Met., 42 (2006) 34–37.

[12] A. Elhebshi, M.S. El-Deab, A. El Nemr, I. Ashour, Corrosion inhibition efficiency of cysteine-metal ions blends on low carbon steel in chloride-containing acidic media, Int. J. Electrochem. Sci., 14 (2019) 3897–3915.

[13] A. Elhebshi, A. El Nemr, M.S. El-Deab, I. Ashour, CBG-HCl as a green corrosion inhibitor for low carbon steel in 0.5 M H_2SO_4 with and without 0.1 M NaCl, Desal. Water Treat., 164 (2019) 240–248.

[14] M.A. Deyab, Effect of cationic surfactant and inorganic anions on the electrochemical behavior of carbon steel in formation water, Corros. Sci. 49 (2007) 2315–2328.

[15] A. El Nemr, A.A. Moneer, A. Khaled, A. El Sikaily, G.F. Elsayed, Modeling of synergistic halide additives effect on the corrosion of aluminum in basic solution containing dye, Mater. Chem. Phys., 144 (2014) 139–154.

[16] A. El Nemr, G.F. El Said, A. Khaled, A. El Sikaily, A.A. Moneer, D.E. Abd-El-Khalek, Differences in corrosion inhibition of water extract of *Cassia fistula* L. pods and *o*-phenanthroline on steel in acidic solutions in the presence and absence of chloride ions, Desal. Water Treat., 52 (2014b) 5187–5198.

[17] I. Ahamad, R. Prasad, M.A. Quraishi, Inhibition of mild steel corrosion in acid solution by Pheniramine drug: experimental and theoretical study, Corros. Sci., 52 (2010) 3033–3041.

[18] C. Verma, L.O. Olasunkanmi, E.E. Ebenso, M.A. Quraishi, Substituents effect on corrosion inhibition performance of organic compounds in aggressive ionic solutions: a review, J. Mol. Liq., 251 (2018) 100–118.

[19] C.M. Fernandes, T.D.S. Ferreira Fagundes, N. Escarpini dos Santos, T. Shewry de M. Rocha, R. Garrett, R.M. Borges, G. Muricy, A.L. Valverde, E.A. Ponzio, *Ircinia strobilina* crude extract as corrosion inhibitor for mild steel in acid medium, Electrochim. Acta, 312 (2019) 137–148.

[20] G. Ji, S. Anjum, S. Sundaram, R. Prakash, *Musa paradisica* peel extract as green corrosion inhibitor for mild steel in HCl solution, Corros. Sci., 90 (2015) 107–117.

[21] I. Rotaru, S. Varvara, L. Gaina, L.M. Muresan, Antibacterial drugs as corrosion inhibitors for bronze surfaces in acidic solutions, Appl. Surf. Sci., 321 (2014) 188–196.

[22] H. Li, S. Zhang, B. Tan, Y. Qiang, W. Li, S. Chen, L. Guo, Investigation of Losartan Potassiumas an eco-friendly corrosion inhibitor for copper in 0.5 M H_2SO_4, J. Mol. Liq., 305 (2020) 112789, doi: 10.1016/j.molliq.2020.112789.

[23] T. Ma, B. Tan, Y. Xu, D. Yin, G. Liu, N. Zeng, G. Song, Z. Kao, Y. Liu, Corrosion control of copper wiring by barrier CMP slurry containing azole inhibitor: combination of simulation and experiment, Colloids Surf., A, 599 (2020) 124872, doi: 10.1016/j.colsurfa.2020.124872.

[24] H.S. Mandour, S.A. Abouel-Enein, R.M.M. Morsi, L.A. Khorshed, Azo ligand as new corrosion inhibitor for copper metal: spectral, thermal studies and electrical conductivity of its novel transition metal complexes, J. Mol. Struct., 1225 (2021) 129159, doi: 10.1016/j.molstruc.2020.129159.

[25] T. Zhao, A. Munis, M. Zheng, J. Hu, H. Teng, L. Wei, 2-(2-Pentadecyl-4, 5-dihydro-1H-imidazol-1-yl) ethanol as a sustainable inhibitor for copper corrosion in molten hydrated phase change materials, J. Mol. Liq., 316 (2020) 113927, doi: 10.1016/j.molliq.2020.113927.

[26] A. Jakab, M.L. Dan, N. Vaszilcsin, Corrosion behaviour of copper in sulphuric acid in the presence of N-methylaniline, Analele Universităţii din Oradea, Fascicula: Protecţia Mediului, 25 (2015) 209–216.

[27] A.H. Tuthill, B. Todd, J. Oldfield, Experience with Copper Alloy Tubing, Waterboxes and Piping in MSF Desalination Plants, Proceedings of World Congress on Desalination and Water Re-use, International Desalination Association (IDA); Cencro de Estudios y Expertmerocion de Obras Pubiicas (CEDEX); Ministerio de Medio Ambiente; Ministerio de Formento; Madrid, Spain, 1997, pp. 251–270.

[28] I.B. Obot, A. Meroufel, I.B. Onyeachu, A. Alenazi, A.A. Sorour, Corrosion inhibitors for acid cleaning of desalination heat exchangers: progress, challenges and future perspectives, J. Mol. Liq., 296 (2019) 111760., doi: 10.1016/j.molliq.2019.111760.

[29] T. Hodgkiess, K.H. Al-Omari, N. Bontems, B. Lesiak, Acid cleaning of thermal desalination plant: do we need to use corrosion inhibitors?, Desalination, 183 (2005) 209–216.

[30] G. Wypych, Methods of Solvent Detection and Testing, Handbook of Solvents, Vol. 2: Use, Health, and Environment, 2019.

[31] A. Jmiai, B. El Ibrahimi, A. Tara, R. Oukhrib, S.J. El Issami, O. Bara, Chitosan as an eco-friendly inhibitor for copper corrosion in acidic medium: protocol and characterization, Cellulose, 24 (2017) 3843–3867.

[32] E.S.H. El Ashry, A. El Nemr, S.A. Essawy, S. Ragab, Corrosion inhibitors Part II: quantum chemical studies on the corrosion inhibitions of steel in acidic medium by some triazole, oxadiazole and thiadiazole derivatives, Electrochim. Acta, 51 (2006) 3957–3968.

[33] E.S.H. El Ashry, A. El Nemr, S.A. Essawy, S. Ragab, Corrosion inhibitors Part IV: quantum chemical studies on the corrosion inhibitions of steel in acidic medium by some aniline derivatives, Indian J. Phys. Proc. Indian Assoc., 1 (2006) 41–62.

[34] E.S.H. El Ashry, A. El Nemr, S.A. Essawy, S. Ragab, Corrosion inhibitors Part III: quantum chemical studies on the efficiencies of some aromatic hydrazides and Schiff bases as corrosion inhibitors of steel in acidic medium, ARKIVOC, xi (2006) 205–220.

[35] E.S.H. El Ashry, A. El Nemr, S.A. Essawy, S. Ragab, Corrosion inhibitors Part V: QSAR of Benzimidazole and 2-substituted derivatives as corrosion inhibitors by using the quantum chemical parameters, Prog. Org., 61 (2008) 11–20.

[36] N.O. Eddy, E.E. Ebenso, A. El Nemr, E.S.H. El Ashry, Quantum chemical study of the inhibition of the corrosion of mild steel in H_2SO_4 by some antibiotics, J. Mol. Model., 15 (2009) 1085–1092.

[37] E.S.H. El Ashry, A. El Nemr, S. Ragab, Quantitative structure activity relationships of some pyridine derivatives as corrosion inhibitors of steel in acidic medium, J. Mol. Model., 18 (2012) 1173–1188.

[38] D. Kumar, V. Jain, B. Rai, Imidazole derivatives as corrosion inhibitors for copper: A DFT and reactive force field study, Corros. Sci., 171 (2020) 108724, doi: 10.1016/j.corsci.2020.108724.

[39] M.M. Solomon, H. Gerengi, T. Kaya, E. Kaya, S.A. Umoren, Synergistic inhibition of St37 steel corrosion in 15% H_2SO_4 solution by chitosan and iodide ion additives, Cellulose, 24 (2017) 931–950.
[40] A.M. Fekry, R.R. Mohamed, Acetyl thiourea chitosan as an eco-friendly inhibitor for mild steel in sulphuric acid medium, Electrochim. Acta, 55 (2010) 1933–1939.
[41] Y. Zhang, B.-L. Liu, L.-J. Wang, Y.-H. Deng, S.-Y. Zhou, J.-W. Feng, Preparation, structure and properties of acid aqueous solution plasticized thermoplastic chitosan, Polymers, 11 (2019) 818, doi: doi: 10.3390/polym11050818.
[42] F. Niola, N. Basora, E. Chornet, P.F. Vidal, A rapid method for the determination of the degree of N-acetylation of chitin-chitosan samples by acid hydrolysis and HPLC, Carbohydr. Res., 238 (1993) 1–9.
[43] K.M. Värum, D. Koga, O. Smidsrød, Degradation of Chitosans, T. Uragami, K. Kurita, T. Fukamizo, Eds., Chitin and Chitosan, Chitin and Chitosan in Life Science, Kodansha Scientific, Tokyo, Japan, 2001, pp. 36–42.
[44] X. Zhao, Z.-Z. Qiao, J.-X. He, Preparation of chitosan biguanidine hydrochloride and application in antimicrobial finish of wool fabric, J. Eng. Fibers Fabr., 5 (2010) 16–24.
[45] H.E. Salama, G.R. Saad, M.W. Sabaa, Synthesis, characterization, and biological activity of cross-linked chitosan biguanidine loaded with silver nanoparticles, J. Biomater. Sci., Polym. Ed., 27 (2016) 1880–1898.
[46] Y.A. Maher, M.E.A. Ali, H.E. Salama, M.W. Sabaa, Preparation, characterization and evaluation of chitosan biguanidine hydrochloride as a novel antiscalant during membrane desalination process, Arabian J. Chem., 13 (2020) 2964–2981.
[47] J. Aldana-González, H. Cervantes-Cuevas, C. Alfaro-Romo, E. Rodriguez-Clemente, J. Uruchurtu-Chavarin, M. Romero-Romo, M.G. Montes de Oca-Yemha, P. Morales-Gil, L.H. Mendoza-Huizar, M. Palomar-Pardave, Experimental and theoretical study on the corrosion inhibition of API 5L X52 steel in acid media by a new quinazoline derivative, J. Mol. Liq., 320 (2020) 114449, doi: 10.1016/j.molliq.2020.114449.
[48] M.A. Quraishi, D. Jamal, Technical note: CAHMT—a new and eco-friendly acidizing corrosion inhibitor, Corrosion, 56 (2000) 983.
[49] M.A. Quraishi, D. Jamal, Corrosion inhibition by fatty acid oxadiazoles for oil well steel (N-80) and mild steel, Mater. Chem. Phys., 71 (2001) 202–205.
[50] I. Felhosi, J. Telegdi, G. Palinkas, E. Kalman, Kinetics of self-assembled layer formation on iron, Electrochim. Acta, 47 (2002) 2335–2340.
[51] I. Felhösi, E. Kálmán, P. Póczik, Corrosion protection by self-assembly, Russ. J. Electrochem., 38 (2002) 230–237.
[52] D.-J. Choi, S.-J. You, J.-G. Kim, Development of an environmentally safe corrosion, scale, and microorganism inhibitor for open recirculating cooling systems, Mater. Sci. Eng., A, 335 (2002) 228–235.
[53] S. Omanovic, S.G. Roscoe, Effect of linoleate on electrochemical behavior of stainless steel in phosphate buffer, Corrosion, 56 (2000) 684–693.
[54] G. Moretti, F. Guidi, G. Grion, Tryptamine as a green iron corrosion inhibitor in 0.5 M deaerated sulphuric acid, Corros. Sci., 46 (2004) 387–403.
[55] G. Shustak, A.J. Domb, D. Mandler, Preparation and characterization of *n*-alkanoic acid self-assembled monolayers adsorbed on 316L stainless steel, Langmuir, 20 (2004) 7499–7506.
[56] K. Aramaki, T. Shimura, Self-assembled monolayers of carboxylate ions on passivated iron for preventing passive film breakdown, Corros. Sci., 46 (2004) 313–328.
[57] S. Ramachandran, B. Tsai, M. Blanco, H. Chen, Y. Tang, W.A. Goddard, Selfassembled monolayer mechanism for corrosion inhibition of iron by imidazolines, Langmuir, 12 (1996) 6419–6428.
[58] A. Mahapatro, D.M. Johnson, D.N. Patel, M.D. Feldman, A.A. Ayon, C.M. Agrawal, Surface modification of functional self-assembled monolayers on 316L stainless steel via lipase catalysis, Langmuir, 22 (2006) 901–905.
[59] A. Raman, M. Dubey, I. Gouzman, E.S. Gawalt, Formation of self-assembled monolayers of alkylphosphonic acid on the native oxide surface of SS316L, Langmuir, 22 (2006) 6469–6472.
[60] A. Raman, E.S. Gawalt, Self-assembled monolayers of alkanoic acids on the native oxide surface of SS316L by solution deposition, Langmuir, 23 (2007) 2284–2288.